Neutron diffraction study of strain and stress induced by thermomechanical fatigue in a single crystal superalloy

2008 J. Phys.: Condens. Matter 20 104255

(http://iopscience.iop.org/0953-8984/20/10/104255)

IOP PUBLISHING JOURNAL OF PHYSICS: CONDENSED MATTER

J. Phys.: Condens. Matter **20** (2008) 104255 (5pp) doi:10.1088/0953-8984/20/10/104255

Neutron diffraction study of strain and stress induced by thermomechanical fatigue in a single crystal superalloy

Erdong Wu[1], Jun Zhang[1], Bo Chen[2], Guangai Sun[2], V Ji[3], D Hughes[4] and T Pirling[4]

[1] Shenyang National Laboratory for Materials Science, IMR CAS, People's Republic of China
[2] Institute of Nuclear Physics and Chemistry, CAEP, People's Republic of China
[3] LEMHE/ICMMO, UMR 8182, Université Paris-Sud 11, 91405 Orsay, France
[4] Institut Laue Langevin, 6 rue Jules Horowitz, 38042 Grenoble, France

Received 16 July 2007, in final form 5 September 2007
Published 19 February 2008
Online at stacks.iop.org/JPhysCM/20/104255

Abstract

The relationship between internal stress and thermomechanical fatigue (TMF) in a Ni-based single crystal superalloy grown along the [001] axis was studied by neutron diffraction. The macroscopic internal stress along the loading axis generally increases with the TMF deformation. However, the internal stress in the precipitate γ' phase increases more significantly than that in the matrix γ phase and contributes more to the stress growth. During the TMF, the stress in the γ' phase is larger than that of the γ phase, thus the γ' phase is stretched whereas the γ phase is compressed along the loading axis. The microstrains in the γ and γ' phases also increase during TMF, but the trend does not follow that of the stresses. The evolutions of the internal stresses and microstrains, and the associated microstructure changes, appear to indicate that the failure by TMF is mostly caused by the residual stress concentration in the hardened γ' phase.

1. Introduction

Owing to the superior mechanical strength and creep resistance at high temperature, Ni-based single crystal superalloys have been widely used for making blades and vanes in advanced industrial gas turbines. The superposition of external load and internal stress associated with microstructure evolutions of dislocation structures and directional coarsening etc has been attributed to the failures of these alloys under various operating conditions [1–3]. The creep, isothermal fatigue (IF) and thermomechanical fatigue (TMF) tests have been the main experiments in simulating the failure processes of the superalloys, and in studying the relationship between the stress states and microstructure evolutions. Since most superalloy components operate under conditions where mechanical load and temperature vary simultaneously, TMF tests could capture important damage micro-mechanisms under varying temperature conditions. However, in comparison with creep and IF, studies on TMF of single crystal superalloys are rather limited [4, 5].

In general, Ni-based superalloys have a composite-like microstructure comprised of fcc matrix (γ) and ordered $L1_2$ structure precipitates (γ'). The internal stress between the two phases plays a very important and complicated role in the failures of the superalloys. There are two main sources of internal stresses, i.e. the internal stresses induced by the crystallographic and thermal expansion misfit between the γ and γ' phases, and those associated with the plastic deformations, especially the dislocation structures. Finite element methods (FEMs) [6, 7] and various experimental techniques [3, 8–10] (mainly diffraction and electron microscopy) have been applied to simulate and measure the internal stress distribution and the associated microstructures in various conditions. The general results suggested that the inter-phase stress parallel (perpendicular) to the loading axis in the γ phase is compressive (tensile) after tensile creep deformation whereas that in the γ' phase is the opposite [8], and the stress state in the γ phase is strongly dependent on the loading axis and that in the γ' phase is inhomogeneous [3, 6].

The present experiments applying the high penetration neutron diffraction technique are to measure the triaxial stress state of a Ni-based single crystal superalloy after TMF and provide numerical information for the future simulation work.

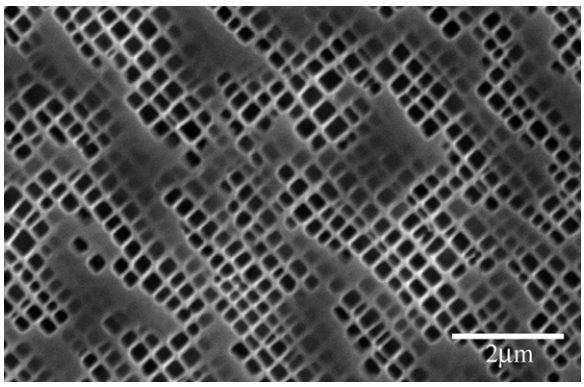

Figure 1. The metallographic microstructure of superalloy after standard heat treatment, the black cubes of precipitate (γ') phase are distributed in the white matrix (γ) phase.

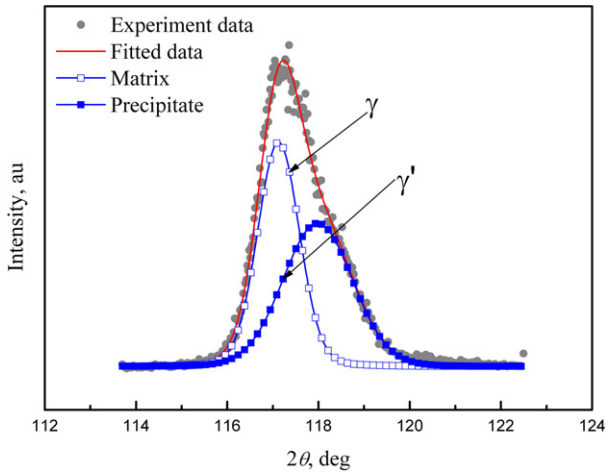

Figure 2. An example of the fitted profile of the (420) diffraction pattern of the 25 TMF cycles sample, indicating the peak separation of the γ and γ' phases based on the intensity ratio.
(This figure is in colour only in the electronic version)

2. Experimental details

2.1. Materials

The Ni-based superalloy investigated in this work is based on a Chinese manufactured superalloy DZ125L with nominal compositions (wt%) of Cr 8.9, Co 9.6, W 6.6, Mo 2.1, Al 4.3, Ti 2.9, Ta 3.4 and balance Ni. The crystallographic orientation of the as-grown single crystal is within 10 °C around the [001] axis. After a standard heat treatment of 1220 °C/2hAC + 1080 °C/4hAC + 900 °C/16hAC, the metallographic microstructure (figure 1) consists of matrix γ and regularly distributed precipitates γ' with an edge length of about 0.45 μm, occupying about 60% of the volume. The single crystals were machined into TMF samples with 8 mm diameter and 26 mm gage length. After machining and before the TMF test, the samples were tempered at 900 °C for 6 h for relieving residual stress.

2.2. Thermomechanical fatigue test

The in-phase (both stress and temperature reach the maximum or minimum at the same time) TMF was conducted under stress control with linear temperature variation on an MTS-810 fatigue test machine. The frequency of the test was 0.005 Hz and the waveform was chosen to be a triangle. The stress varied from 0 to 700 MPa (77% of the yielding stress at room temperature) and the temperature varied from 450 to 900 °C. The loading axis was parallel to the crystal growth direction [001]. The failure life was defined as the number of cycles at which the sample was broken (203 cycles). Accordingly, another four samples, 3/4 (150 cycles, necked), 1/2 (100 cycles), 1/4 (50 cycles) and 1/8 (25 cycles) failure life, were prepared. The unloaded samples were air cooled and removed from the equipment.

2.3. Neutron diffraction measurements

Neutron diffraction experiments were performed on the neutron strain analyzer SALSA at ILL (Grenoble, France) equipped with an area detector and an additional Euler cradle on the hexapod sample stage. The wavelength of neutron radiation is 1.36 Å. The measurements were focused on the center of the samples in a volume of 3 mm^3 defined by the slits, except for the 100 cycle sample, where an additional location 5 mm away from the central point on the loading axis was also measured.

The triaxial stress state of a macroscale point of a cubic single crystal is defined by six independent tensors, which can be derived from the corresponding strain tensors by matrix transitions according to Hook's law. Therefore, at least six interplanar spacings (d_{hkl}) of different planes (among them at least one plane has to be unrelated) are required to determine the six independent strain tensors [9]. Accordingly, seven or eight diffraction patterns from two different reflection plane families of {331} and {420} were measured and analyzed for each measurement location. As the γ and γ' phases have similar structures and lattice parameters, and their reflections are nearly overlapped, the separation of the reflections of the two phases was performed on the constraint of a fixed intensity ratio $I_\gamma/I_{\gamma'}$ of 1/1.05 for the γ and γ' phases, respectively, obtained from the composition and volume contributions of the two phases [11]. The reflections are fitted by a Voigt profile (figure 2). The internal stress states and microstrains of the γ and γ' phases were calculated from the measured d_{hkl} and full width at half maximum (FWHM) from the fittings respectively.

2.4. Calculations of stress

Unlike calculation of the plane stress state [12], an additional unstressed interplanar spacing (d_0) derived from an unstressed sample is essential for the calculation of the triaxial stress state. Normally, the tempered sample without a TMF test can be considered as unstressed. However, due to intrinsic lattice misfit between the γ and γ' phases, existence of considerable misfit stress is unavoidable in the tempered sample [13], thus reliable values of triaxial internal stress cannot be derived in this way. To overcome this problem, the following

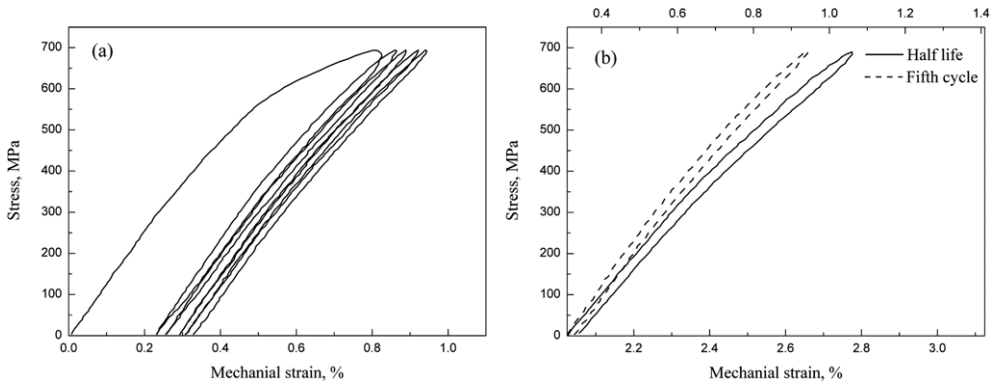

Figure 3. The stress–strain curves of the TMF test: (a) the first five cycles; (b) the fifth cycle and the 100th cycle, corresponding to the upper and lower strain scales, respectively.

treatment [14] was applied: a triaxial stress tensor σ_{ij} can be separated into two components, a hydrostatic stress τ_{H} and a deviatoric stress τ_{ij}:

$$\sigma_{ij} = \delta_{ij}\tau_H + \tau_{ij}, \tag{1}$$

where δ_{ij} is a component of the δ function and $\tau_H = (\sigma_{11} + \sigma_{22} + \sigma_{33})/3$. Based on symmetrical deformation, it is assumed that $\tau_{010} = \tau_{100} = -\tau_{001}/2$, where τ_{010}, τ_{100} and τ_{001} represent the deviatoric stress tensors along the [010], [100] and [001] directions, respectively. It is suggested that as a scalar the hydrostatic stress reflects the volume change and is strongly affected by a deviation in d_0, whereas the deviatoric stress reflects the evolution of the internal stress and is not sensitive to d_0 [14]. Therefore, the derivation of the deviatoric tensor will provide some reliable quantitative information on the internal stress state for a superalloy during the mechanical deformation.

The macrostress tensor ${}^{\mathrm{M}}\sigma_{ij}$ can be calculated from the stress tensors of the γ and γ' phases by

$${}^{\mathrm{M}}\sigma_{ij} = f^{\gamma} \cdot {}^{\gamma}\sigma_{ij}^{t} + f^{\gamma'} \cdot {}^{\gamma'}\sigma_{ij}^{t}, \tag{2}$$

where ${}^{\gamma}\sigma_{ij}^{t}$ and ${}^{\gamma'}\sigma_{ij}^{t}$ are the total stress of the γ and γ' phases, respectively, and f^{γ} and $f^{\gamma'}$ are the volume fractions of the γ and γ' phases, respectively which are calculated from the measured d_{hkl} of the two phases illustrated in figure 2. The mechanical behavior of a superalloy will be the consequence of the interaction between the γ and γ' phases. Based on the strain continuity on the interface of the γ and γ' phases, the secondary inter-phase stresses ${}^{\gamma}\sigma_{ij}^{\mathrm{II}}$ and ${}^{\gamma'}\sigma_{ij}^{\mathrm{II}}$ in γ and γ' phases can be calculated respectively by [14]

$$\begin{aligned} {}^{\gamma}\sigma_{ij}^{\mathrm{II}} &= f^{\gamma'}({}^{\gamma}\sigma_{ij}^{t} - {}^{\gamma'}\sigma_{ij}^{t}) \\ {}^{\gamma'}\sigma_{ij}^{\mathrm{II}} &= f^{\gamma}({}^{\gamma'}\sigma_{ij}^{t} - {}^{\gamma}\sigma_{ij}^{t}), \end{aligned} \tag{3}$$

The relations in (3) are valid for both triaxial and deviatoric stress tensors. The elastic constants of the γ and γ' phases used in the calculation were as follows: γ, $C_{11} = 218.5$ GPa, $C_{12} = 117.4$ GPa, $C_{44} = 143.4$ GPa; γ', $C_{11} = 166.9$ GPa, $C_{12} = 89.7$ GPa, $C_{44} = 109.5$ GPa [15].

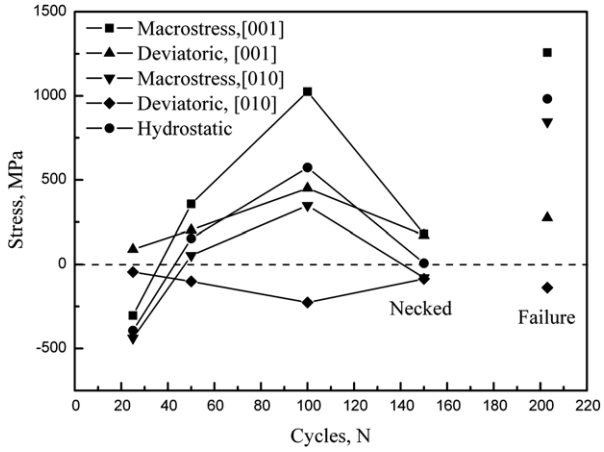

Figure 4. The changes of the triaxial macrostress, its hydrostatic and deviatoric components along directions [001] and [100] versus TMF cycles, respectively.

3. Results

3.1. Thermomechanical test

Figure 3(a) shows a typical cyclic stress–strain curve of the first five TMF cycles. It can be seen that the sample has yielded at the first cycle, but become hardened after the first cycle and slightly softened afterwards. In comparison with the tensile peak strain of 0.62% at the fifth cycle, the strain at the half failure life is 0.75% (see figure 3(b)). Therefore, the TMF test simulated a superalloy component through an overload operating condition, and revealed the corresponding internal stress change and failure mechanism.

3.2. Macro stress

Figure 4 shows the relationship between TMF cycle and the triaxial macrostress, and its hydrostatic and deviatoric components along the [001] and [010] directions. As the sample has necked at 150 cycles, the stress data at the failure (203 cycles) have become irrelevant, and are only displayed for reference. It can be seen that the triaxial macrostress tensors derived from the d_0 of the tempered sample either along the

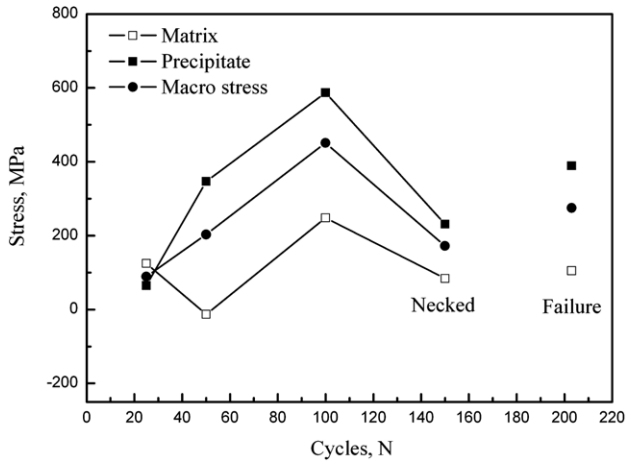

Figure 5. Deviatoric stress components of the γ and γ' phases along the [001] direction versus TMF cycles. The macrostress is also presented for comparison.

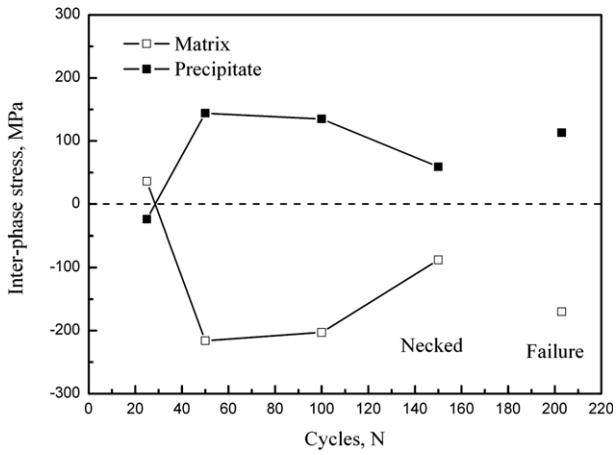

Figure 6. The inter-phase stress of the γ and γ' phases along the loading axis [001] versus TMF cycles.

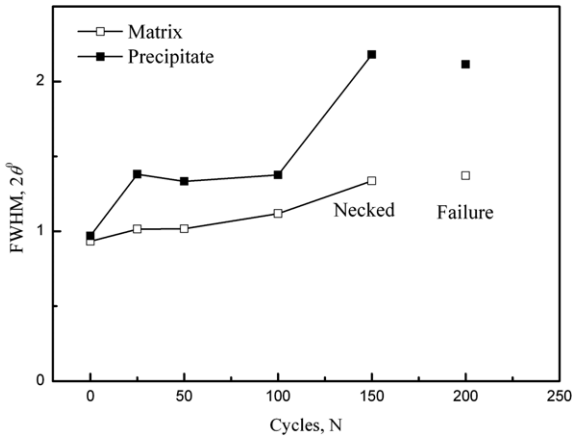

Figure 7. The average of FWHM of the {420} planes in γ and γ' phases versus TMF cycle.

loading axis [001] or along axis [010] have increased with the TMF deformation unilaterally until the sample necked, with the maximum stress reaching an unrealistic level above the yielding stress. The hydrostatic values showed a similar trend, but the deviatoric stresses behaved slightly differently, exhibiting the trend of a moderate stress increase along the [001] axis. The diagram clearly indicates that if a significant error in d_0 is inherited by the triaxial macrostress, it would be strongly reflected by the hydrostatic stress, but would less affect the deviatoric stress.

The macrostress data of the 100 cycle sample for the location 5 mm away from the central point along the loading axis have shown a significant reduction from that of the central position. The deviatoric component along [001] reduced from 450 MPa to a negative value of −50 MPa. Though the basic trend of the macrostress change is consistent with the smaller temperature deviations during TMF cycles at this location, the extension of the stress concentration and variation has been unexpectedly high. The results indicate that the TMF tests would cause a significant inhomogeneous distribution and concentration of the macrostress in the sample. As the positioning accuracy of the measurement is ∼1 mm, the uncertainty in the internal stress data would be at a relatively high level of 100 MPa, which can be considered as the uncertainty of the relevant stress plots.

3.3. Inter-phase stress

The changes of the deviatoric stresses of γ and γ' phases along the [001] axis are shown in figure 5. The results indicate that the stress in the γ' phase is always larger than that of the γ phase along the loading axis. This relation is also retained at the location 5 mm away from the central point for the 100 cycle sample, though the total stresses of the γ and γ' phases were reduced significantly. Based on (3), the deviatoric components of the inter-phase stress of the γ and γ' phases along the loading axis are calculated and shown in figure 6. The results suggest that during the development of TMF, the precipitate γ' phase is stretched, whereas the matrix γ phase is compressed along the loading axis. Accordingly, the inter-phase stress behaves in the opposite way along the [010] or [100] axis. This inter-phase stress relation is consistent with that observed in the creep test of the superalloys [8], and agrees well with the internal stress model of the two phases undergoing tension load proposed by Mughrabi [16].

3.4. Microstrains

The internal stress is based on the elastic strain of the crystal lattice, and is measured by the shift of the diffraction line, whereas the microstrain may reflect the plastic deformation of the crystal lattice, and is proportional to the broadening of the diffraction line. Figure 7 illustrates the relationship between microstrain presented by FWHM and the TMF cycles, and shows a trend of increasing microstrain with TMF. However, the microstrain of the γ' phase is much higher than that of the γ phase, and the increase primarily occurs during the earlier cycles (at 25 cycles, the microstrain in the necked sample is not considered), which does not follow the evolution of the internal stress. The increases of the microstrain were often associated with evolution of dislocation structures in the crystal

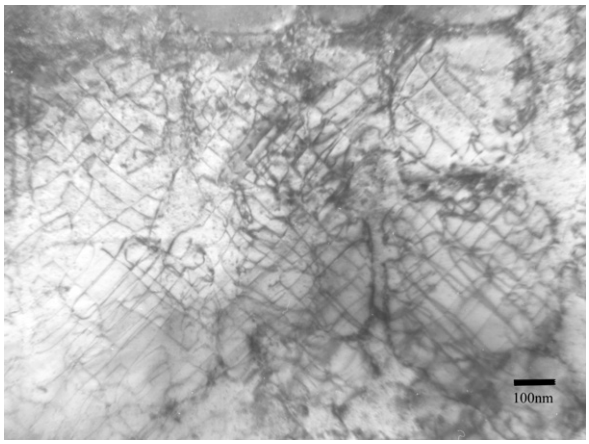

Figure 8. The dislocation structures observed on the TMF sample after 50 TMF cycles, side case, and the diffraction vector $g = 020$.

lattice [17, 18]. The TEM photograph of the superalloy after 50 TMF cycles has shown the intensive distribution of the dislocation networks in the γ' phase (see figure 8). This kind of dislocation structure has also been observed in a similar superalloy sample after the IP TMF [4].

4. Discussions

All the above observations have indicated that the dislocation structures evolved in the γ' phase during TMF are responsible for the increased microstrain and internal stress in the superalloy during TMF. The appearances of intensive dislocation structures and interrelated microstrains in the γ' phase during the initial stage of the TMF is likely to be associated with the remarkable plastic deformation and hardening of the sample observed in this period. The internal stress will build up in the jammed dislocation network of the hardened γ' phase during further TMF, reside there after unloading and lead to cracking and failure of the sample, and this assumption is consistent with the observed increase of internal stress with TMF. The observed tensile stress of the γ' phase at room temperature agrees with a hard γ' phase during TMF. This phenomenon is contradictory to the fact that in this type of superalloy the γ' phase is softer than the γ phase at room temperature, and only becomes opposite at elevated temperature [15], therefore further confirming the hardening of the γ' phase during the TMF test. It appears that the stress build-up and concentration in the hardened γ' phase attribute the most to the failure of the structures under the overload TMF test.

5. Conclusions

The internal stress state of a Ni-based single crystal superalloy containing γ and γ' phases after TMF test was measured by neutron diffraction. The measurements provide some quantitative TMF induced stress and strain information for the future simulation studies.

(1) The macroscopic internal stress is highly concentrated and inhomogeneous, and generally increases with the TMF deformation. However, the internal stress in the precipitate γ' phase increases more significantly than that in the matrix γ phase along the loading axis.
(2) The internal stress in the γ' phase is larger than that of the γ phase during evolution of TMF, thus the γ' phase is tensile whereas the γ phase is compressive along the loading axis. The trend of the inter-phase stress on TMF agrees with the proposed stress model.
(3) The microstrains in the γ and γ' phases increase during TMF, but the trend does not follow that of the stresses. The evolutions of the internal stresses and microstrains, and the associated microstructure changes, appear to indicate that the failure by TMF is mostly caused by the development of dislocation structures related to hardening and associated stress build-up and concentration in the γ' phase.

Acknowledgments

We appreciate the assistance of J Zhang, L H Lou, J L Wen and G Yao of IMR in the experiments. E Wu acknowledges the beam time and associated facilities provided by ILL, and the traveling assistance provided by the Chinese Spallation Neutron Source (CSNS).

References

[1] Veron M, Brechet Y and Louchet F 1996 *Acta Mater.* **44** 3633
[2] Brien V, Kubin L P and Decamps B 2001 *Phil. Mag.* A **81** 2285
[3] Lu Z, Pyczak F, Biermann H and Mughrabi H 2002 *Phil. Mag.* A **82** 1219
[4] Liu F, Wang Z G, Ai S H, Wang Y C, Sun X F, Jin T and Guan H R 2003 *Scr. Mater.* **48** 1265
[5] Liu F, Wang Y C, Zhang H, Ai S H and Wang Z G 2003 *Mater. Sci. Technol.* **19** 853
[6] Muller L, Glatzel U and Fellerkniepmeier M 1993 *Acta Metall. Mater.* **41** 3401
[7] Zhou L, Li S X, Chen C R, Wang Y C, Zang Q S and Lu K 2003 *Mater. Sci. Eng.* A **352** 300
[8] Kuhn H A, Biermann H, Ungar T and Mughrabi H 1991 *Acta Metall. Mater.* **39** 2783
[9] Marty B, Motetto P, Gergaud P, Lebrun J L, Ostolaza K and Ji V 1997 *Acta Mater.* **45** 791
[10] Von Grossmann B, Biermann H, Tetzlaff U, Pyczak F and Mughrabi H 2000 *Scr. Mater.* **43** 859
[11] Ma S, Rangaswamy P and Majumdar B S 2003 *Scr. Mater.* **48** 525
[12] Zhang J, Wang S C, Wu E, Zhang J and Lou L H 2007 *Acta Metall. Sin.* **43** 1161
[13] Pollock T M and Argon A S 1994 *Acta Metall. Mater.* **42** 1859
[14] Winholtz R A and Cohen J B 1992 *Mater. Sci. Eng.* A **154** 155
[15] Ganghoffer J F, Hazotte A, Denis S and Simon A 1991 *Scr. Metall. Mater.* **25** 2491
[16] Mughrabi H 1983 *Acta Metall.* **31** 1367
[17] Metzger T, Hopler R, Born E, Ambacher O, Stutzmann M, Stommer R, Schuster M, Gobel H, Christiansen S, Albrecht M and Stunk H P 1998 *Phil. Mag.* A **77** 1013
[18] Wu E, Kisi E H and Gray E M A 1998 *J. Appl. Crystallogr.* **31** 363